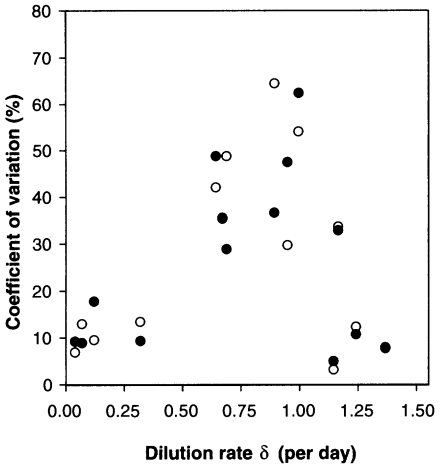

Fig. 3. Relative stability of experimental predator-prey chemostat cultures. Coefficient of variation (*23*) of time series (day 20 to end of trial) for all chemostat trials at N_i = 80 μmol/liter. Low CV indicates populations at equilibrium (CV > 0 because of noise), high CV indicates fluctuating populations. *Brachionus calyciflorus* (predator, black symbols) and *C. vulgaris* (prey, open symbols).

plains the overall dynamical behavior of the nitrogen-*Chlorella-Brachionus* system; a simple laboratory culture system containing populations of real predators and prey exhibits the oscillatory dynamics predicted by a mathematical model. This model is of the same type that has led theoreticians to posit that fluctuations in natural populations may be internally driven (*24*). However, the model does not correctly predict some of the quantitative characteristics: the observed cycle periods are too long, and the positions of the predator minima and prey maxima are too close together relative to prediction. This suggests that some additional mechanism, not represented in our model (e.g., variable algal quality), comes into play only when the populations are undergoing large-amplitude cycles.

The rotifer-algal chemostat system has allowed us to study the conditions under which predator-prey cycles arise. It now provides an opportunity to explore the occurrence of more complex dynamics such as deterministic chaos (*20–22*), cyclic predator-prey coevolution (*25*), and evolutionary responses that might reduce the likelihood of complex dynamics (*26*).

References and Notes

1. M. L. Rosenzweig, *Science* **171**, 385 (1971).
2. A. Hastings, T. Powell, *Ecology* **72**, 896 (1991).
3. K. McCann, A. Hastings, G. R. Huxel, *Nature* **395**, 794 (1998).
4. C. S. Elton, M. Nicholson, *J. Anim. Ecol.* **11**, 215 (1942).
5. L. S. Luckinbill, *Ecology* **54**, 1320 (1973).
6. J. L. Jost, J. F. Drake, A. G. Fredrickson, H. M. Tsuchiya, *J. Bacteriol.* **113**, 834 (1973).
7. J. L. Jost, J. F. Drake, H. M. Tsuchiya, A. G. Fredrickson, *J. Theor. Biol.* **41**, 461 (1973).
8. V. E. Dent, M. J. Bazin, P. T. Saunders, *Arch. Microbiol.* **109**, 187 (1976).
9. R. F. Constantino, J. M. Cushing, B. Dennis, R. A. Desharnais, *Nature* **375**, 227 (1995).
10. E. McCauley, R. M. Nisbet, W. W. Murdoch, A. M. DeRoos, W. S. C. Gurney, *Nature* **402**, 653 (1999).
11. U. Halbach, *Oecologia* **4**, 176 (1970).
12. M. E. Boraas, *Am. Soc. Limnol. Oceanogr. Spec. Symp.* **3**, 173 (1980).
13. We established cultures of *C. vulgaris* (UTEX no. 26) and *B. calyciflorus* in 380-ml glass chemostats at 25° ± 0.3°C and constant fluorescent illumination at 120 ± 20 μE/m² per second. A continuous flow of sterile medium was pumped through the chemostats; sterile air was bubbled continuously both to prevent CO_2 limitation of the algae and to enhance mixing. We removed algal growth from the inner walls of the vessels daily. Our medium (pH = 6.8 ± 0.4) contained nitrate at concentrations that limited algal growth, plus nonlimiting concentrations of other nutrients, trace metals, and vitamins.
14. Trials were started by adding *B. calyciflorus* to a chemostat culture of *C. vulgaris* and lasted between 16 and 120 days. We sampled daily (using hypodermic syringes; 0.457-mm needle) through ports near bottom and top of each chemostat. Entire samples were counted for rotifers under a dissecting microscope. Samples of algae preserved in Lugol's solution were counted using either a compound microscope or a particle counter (CASY 1, Schärfe, Germany). We detected no systematic overrepresentation of organisms in either the top or bottom samples. All data on organismal concentrations are means of duplicate samples.
15. Because our data suggest that the rotifers become senescent as they age (fecundity decreases although food uptake remains unchanged), we introduced a fecundity decay rate (λ), and a variable (*B*) for the total concentration of (reproducing and nonreproducing) rotifers (*R* includes only reproducing rotifers).
16. C. S. Holling, *Can. Entomol.* **91**, 293 (1959).
17. S. Aoki, A. Hino, *Fisheries Sci.* **62**, 8 (1996).
18. We parameterized our model with b_C = 3.3 per day; K_C = 4.3 μmol/liter (*27*); b_B = 2.25 per day; K_B = 15 μmol/liter [from nonlinear regression of data on functional response in (*28*)]; m = 0.055 per day; λ = 0.4 per day; ε = 0.25 (*17*). We took b_C to be the highest δ at which *Chlorella* can maintain a stable population in the chemostat in the absence of rotifers and estimated b_B from data for exponentially growing *Brachionus* under high algal density. We used counts of dead rotifers from chemostat cultures to determine m. Counts of subitaneous eggs per rotifer provided estimates for fecundity and λ. *N*, *C*, *R*, and *B* are modeled as moles of nitrogen and then converted to numbers of organisms [1 μmol/liter of *Chlorella* = 5 × 10⁴ cells per milliliter (*12*); 1 μmol/liter of *Brachionus* = 5 females per milliliter (*12*)].
19. R. M. Nisbet, A. Cunningham, W. S. C. Gurney, *Biotech. Bioeng.* **25**, 301 (1983).
20. M. Kot, G. S. Sayler, T. W. Schultz, *Bull. Math. Biol.* **54**, 619 (1992).
21. A. Gragnani, O. De Feo, S. Rinaldi, *Bull. Math. Biol.* **60**, 703 (1998).
22. S. H. Strogatz, *Nonlinear Dynamics and Chaos* (Addison-Wesley, Reading, MD, 1994).
23. To avoid misinterpretation of trials with low *Brachionus* density, CVs were adjusted by subtracting the CV due to measurement error, which was estimated from duplicate measurements (*14*). On average the CV was reduced to 78% (*Chlorella*) and 59% (*Brachionus*) of its unadjusted value.
24. R. M. May, *Science* **177**, 900 (1972).
25. A. I. Khibnik, A. S. Kondrashov, *Proc. R. Soc. London Ser. B* **264**, 1049 (1997).
26. S. Ellner, P. Turchin, *Am. Nat.* **145**, 343 (1995).
27. R. Tischner, H. Lorenzen, *Planta* **146**, 287 (1979).
28. U. Halbach, G. Halbach-Keup, *Arch. Hydrobiol.* **73**, 273 (1974).

29. M. Boraas and C. Kearns provided advice on chemostat setup and M. Boraas gave us a culture of *B. calyciflorus*. G. Heber performed extensive numerical simulations for Fig. 1 on the AC³ Velocity complex of the Cornell Theory Center (funded by Cornell University, New York State, federal agencies, and corporate partners). R. Babcock, K. Brewer, K. Check, C. Cline, L. Davias, A. Holmes, P. Kalika, M. Kalvestrand, and A. Katholos helped sample and maintain the chemostats. J. Fieberg, C. Kearns, D. Post, L. Puth, J. Rowell, N. Thomson, N. Tisch, C. Webb, and two anonymous referees made helpful comments on the manuscript. Funded by the Andrew Mellon Foundation.

4 August 2000; accepted 18 September 2000

Coherence and Conservation

David J. D. Earn,[1]* Simon A. Levin,[2] Pejman Rohani[3]

A principal aim of current conservation policy is to reduce the impact of habitat fragmentation. Conservation corridors may achieve this goal by facilitating movement among isolated patches, but there is a risk that increased connectivity could synchronize local population fluctuations (causing coherent oscillations) and thereby increase the danger of global extinction. We identify general conditions under which populations can or cannot undergo coherent oscillations, and we relate these conditions to local and global extinction probabilities. We suggest a simple method to explore the potential success of conservation corridors and, more generally, any manipulations of dispersal patterns that aim to protect threatened species or control pests.

There is growing concern about the adverse effects of habitat fragmentation on the long-term viability of endangered species (*1*). Many studies attempt to evaluate the effects of past actions, to predict the outcomes of further fragmentation, and to promote conservation measures (*2, 3*).

A critical issue that is often emphasized is synchrony of population dynamics in different habitat patches (*4–9*). If a population goes extinct in one patch while other patches retain substantial numbers, the classical "rescue effect" can prevent global extinction (*7*). However, if extinction occurs in all patches

[1]Department of Mathematics and Statistics, McMaster University, Hamilton, Ontario, Canada, L8S 4K1. [2]Department of Ecology and Evolutionary Biology, Princeton University, Princeton NJ, 08544 USA. [3]Department of Zoology, University of Cambridge, Downing Street, Cambridge CB2 3EJ, UK.

*To whom correspondence should be addressed. E-mail: earn@math.mcmaster.ca

simultaneously, then "rescue" is impossible. Consequently, spatial coherence (synchrony) of population dynamics may be dangerous for species that we wish to conserve.

A strategy that is the source of continuous debate is the preservation or construction of "conservation corridors," i.e., pathways that make it possible (or easier) for individuals to move among habitat patches (*10, 11*). Corridors may have the desired effect of promoting rescues. Unfortunately, they may instead have the undesired effect of synchronizing periods of low population density in different patches, making the population as a whole more susceptible to "bad years," demographic stochasticity, and Allee effects (*12, 13*). The long-term effects of conservation corridors are therefore uncertain.

Here, we describe a way to make quantitative predictions about the success of conservation corridors and, more generally, policies that affect movement patterns of endangered species. For any given dispersal behavior, we can determine the likelihood of synchronous fluctuations in species abundances and the corresponding probabilities of local and global extinction. We illustrate our results using a simple spatial population model and then explain general coherence criteria that can be applied to realistic models and real ecological systems.

Our illustrative model (*14*) consists of a single species with discrete generations and 10 suitable habitat patches. Within each patch, reproduction is density-dependent, and the maximum fecundity in any generation is r [specifically, the reproduction function is the logistic map (*14*)]. A fraction m of individuals migrates before reproducing. We consider two patterns of migration: equal coupling (i.e., dispersing individuals are equally likely to move to any of the other patches) and nearest neighbor coupling (i.e., dispersers move only to adjacent patches). Realistic dispersal patterns (*15*) typically lie somewhere between these extremes.

We first examine when coherent oscillations (*16*) are impossible, possible, or inevitable for our illustrative logistic metapopulation. In Fig. 1, if the reproductive and dispersal rates (r, m) lie inside the blue "coherence impossibility region," then coherent oscillations will never occur; even the slightest perturbation from coherence will grow and the system will become incoherent (different patches will settle on different sequences of population densities). Outside the blue region, sufficiently small perturbations will not disrupt coherent oscillations. If (r, m) lies in the red "coherence inevitability region," then coherence is unavoidable. If (r, m) lies in the unshaded region (neither blue nor red), then coherent oscillations may or may not occur, depending on the initial state. Because the coherence regions are very different in the two panels of Fig. 1, it is clear that quantifying the dispersal pattern is crucial when estimating the susceptibility of a system to coherent oscillations (and, in turn, the effects of a network of corridors on extinction probabilities). The blue and red regions can be estimated with numerical simulations; we determined them exactly from analytical criteria, which we describe below.

On each panel of Fig. 1, we superimposed the bifurcation diagram for the logistic map, which summarizes the single-patch dynamics as a function of fecundity (e.g., a single point above a given r value indicates abundance is in equilibrium, two points indicate alternating highs and lows, and a broad band of points indicates chaos). This bifurcation diagram shows that for our illustrative model, coherence is always possible in the nonchaotic regime (the probability of coherence may be small, but it is never strictly zero if $r \lesssim 3.57$).

Between the extremes of impossibility and inevitability, coherent dynamics occur with some nonzero probability, which is a function of both r and m. The top two panels of Fig. 2 show the probability that the dynamics are coherent to within 10% after 10 years (starting from random initial conditions). The risk of coherence is typically larger for smaller r and larger m, but the details depend on the dispersal pattern. Real systems are always subject to demographic and environmental stochasticity. Extensive simulations (*17*) show that moderate levels of stochasticity do not substantially affect the probability of spatial coherence. In particular, the center and bottom panels of Fig. 2 show that our calculations of coherence probabilities are robust to variance in patch quality and to local environmental noise.

When coherent oscillations are improbable, global extinction is less likely than extinctions in individual patches. Figure 3 verifies this for our illustrative logistic metapopulation in the presence of global noise (randomly occurring events that affect all patches equally). Extinction probabilities are given by the frequency of zero population size (*18*). After local extinctions, dispersal from other patches leads to colonization of empty patches.

Drops in the global extinction rate (compared with the local extinction rate) correspond closely to drops in the probability of coherence (green in Fig. 3) and not to the transition from regular to chaotic dynamics. Thus, persistence is determined principally by susceptibility to coherence rather than by the nature of the dynamics (nonchaotic or chaotic). Theoretical population ecologists have sought to find a link between chaos and population persistence (*19, 20*). Our results show that there is nothing special about chaos in this respect: Low probabilities of coherence (and hence global extinction) can occur when the single-patch dynamics are very simple. The global extinction probability is generally lower if there is a wide range of possible population densities; this occurs in the chaotic regime for the logistic map but is not a general feature of chaos (*21*).

Our results for the logistic metapopulation model can be derived from analytical criteria that apply generally (not just to this specific example). The criteria can be formulated in terms of three ecologically determined quan-

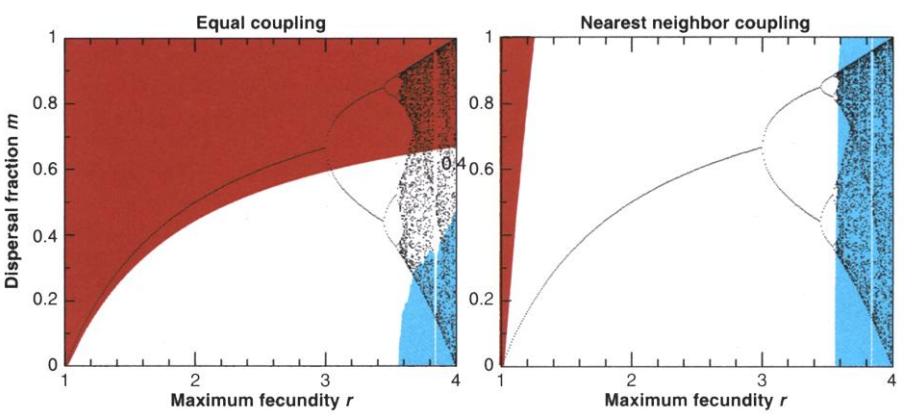

Fig. 1. Possibility and inevitability of coherence in a simple metapopulation model (10 coupled logistic maps) as functions of maximum fecundity (r) and the fraction of the population that disperses (m). The graphs are superimposed on the bifurcation diagram for the logistic map to emphasize the underlying dynamics of the single-patch map. In each panel, the coherence impossibility region is shaded in blue (coherent oscillations are impossible within it and possible outside it). The boundary is derived in each case from criterion 1; for equal coupling (left), $\lambda = 1 - [n/(n-1)]m$, whereas for nearest neighbor coupling on a ring (right) $\lambda = 1 - [1 - \cos(2\pi/n)]m$. The lack of smoothness of the boundary of the blue region arises because coherence is stable locally (in phase space) in all of the periodic windows of the logistic map. The coherence inevitability region derived from criterion 3 is shaded in red. Inside this region, coherent oscillations are inevitable, regardless of initial conditions. Between the blue region and the red region, coherent oscillations may or may not occur (see Fig. 2).

tities: (i) λ, a statistic that characterizes the influence of the dispersal pattern on the susceptibility of the system to coherent oscillations. In our illustrative example, λ is a function of two ingredients, the proportion of individuals that disperse (m) and the type of coupling (equal or nearest neighbor). Technically, λ is the subdominant eigenvalue (*22*) of the dispersal matrix (*15*). (ii) μ, a measure of the average reproductive rate within a patch. Technically, μ is the Lyapunov exponent (*23*) associated with a single patch. This number has been proposed as a formal definition of fitness (*24*). (iii) r, the maximum fecundity or maximum reproductive rate within a patch. The analytical criteria (*25*) are the following. If

$$e^{\mu}|\lambda| < 1 \quad (1)$$

then coherent oscillations are possible. If

$$e^{\mu}|\lambda| > 1 \quad (2)$$

then coherent oscillations will never occur. Finally, if

$$r|\lambda| < 1 \quad (3)$$

then coherent oscillations are inevitable, regardless of the initial state of the system. In Fig. 1, the (blue) coherence impossibility region is determined by condition 2, whereas the (red) coherence inevitability region is determined by condition 3.

In the past, a few special cases of the local criterion 1 have been obtained for specific models (*26–30*). Criteria 1 and 2 generalize these previous results, providing conditions that are much more useful because they are model independent. However, as the logistic metapopulation example showed, formal local stability of coherence is not sufficient to guarantee coherence in practice; the probability of coherence is often negligible in parameter regions where coherence is technically locally stable. This highlights the importance of the global criterion 3; if condition 3 is satisfied, then coherence is inevitable and substantial extinction risk may be unavoidable. As far as we are aware, this global condition has never been stated previously, even for a specific model.

We emphasize that the "logistic metapopulation model" that we used for the figures is merely an illustrative example (*31*). Our derivations (*25*) of criteria 1, 2, and 3 apply equally well to reproduction functions other than the logistic, including those that incorporate an Allee effect (*12, 13*), and the approach can be used for organisms that reproduce continuously. It also applies to multispecies interactions, situations where there are time delays (due to age or stage structure, for example), and systems that are subject to seasonal forcing or other explicitly time-dependent external factors (*32*). For such systems, μ and r must be generalized (*32*), but the forms of criteria 1, 2, and 3 are unchanged.

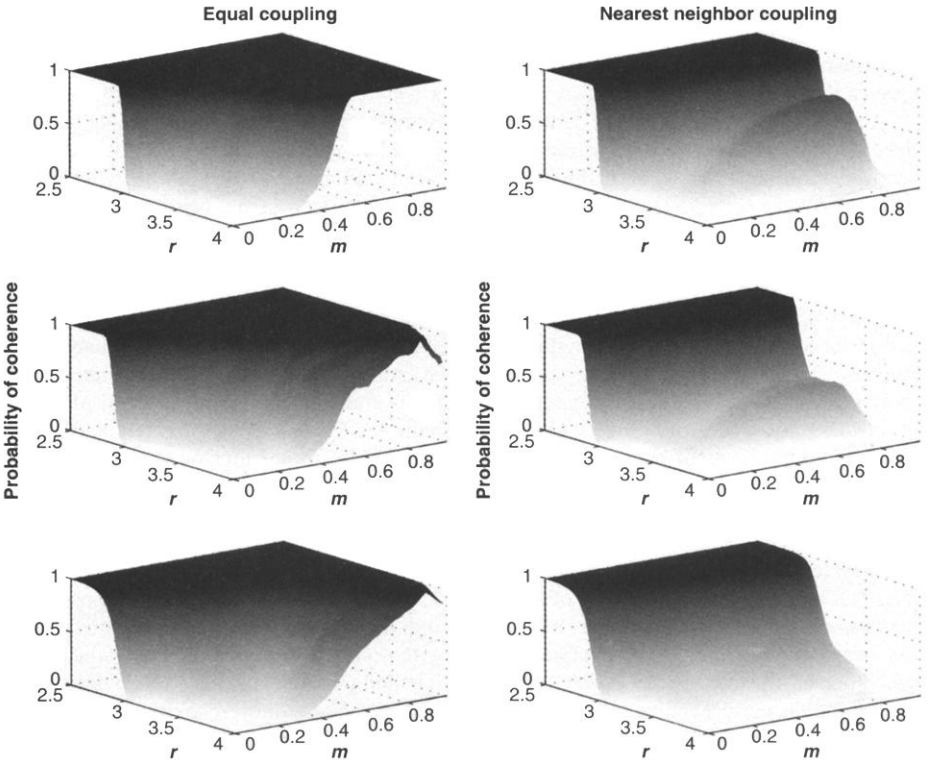

Fig. 2. Risk of coherence. In each panel, the height of the surface gives the probability of coherence to within 10% after 10 iterations of the logistic metapopulation model, based on a random sample of 10,000 initial conditions for each pair of parameter values (r, m). We use a crude definition of coherence (10%) and a rapid time to coherence (10 years) because such crude measures would have to be applied to real systems. The probability surfaces are similar if we require coherence to within 1% after 100 or 1000 iterations, indicating that relaxation to coherence is not substantially affected by supertransient behavior (*43*). The two center panels explore the effects of variance in patch quality: The maximum fecundity is different in each patch [$r_i = r \times (1 + \alpha_i)$, where $\alpha_i \in \{-0.05, -0.04, \ldots, 0.05\}$]. The bottom two panels explore the effects of local environmental noise: Each year the maximum fecundity in patch i is $r_i^t = r \times (1 + z^t)$, where z^t is normally distributed with mean zero and standard deviation 0.025. In both the center and bottom panels, the level of patch variance or stochasticity is large relative to our coherence threshold of 10%, showing that our results are robust to these factors.

We noted for the logistic metapopulation that coherence is always possible (although not necessarily very likely) in the nonchaotic regime. In fact, it is true in general that coherent fluctuations in abundance are always possible if the underlying single-patch dynamics are equilibrial, cyclical, or quasi-periodic (*33*).

Any given model has associated values of λ, μ, and r, which can be inserted in our coherence criteria. Moreover, empirical estimates of λ, μ, and r can be used in these criteria without reference to any specific model. Thus, conditions 1, 2, and 3 can be used directly to evaluate ecological data.

To make direct use of criteria 1, 2, and 3 in a given conservation setting, we need estimates of μ and r and, most crucially, the dispersal pattern, from which we can compute λ. These numbers will always be difficult to determine from field data (*34, 35*), but, fortunately, estimating them does not require us to tie ourselves to any particular model. To evaluate the impact of a network of conservation corridors, we need to estimate the difference in λ with and without the corridors. This difference in λ translates, through criteria 1, 2, and 3, into a difference in susceptibility to coherent oscillations (which in turn influences the danger of global extinction).

We suggest that estimating changes in λ due to conservation measures will be useful even if μ and r cannot be reliably determined from existing data; such estimates could form a valuable component of qualitative assessments of conservation proposals. If the difference in λ that can be achieved is relatively small, then the contribution of rescue effects to extinction probabilities will generally not be strongly affected (*36*). This rough assessment based on analytical criteria can always be supplemented by detailed investigation of extinction probabilities in a variety of realistic models, with the simple numerical technique (*18*) that we applied to produce Fig. 3; extinction probabilities in such models should be computed for the range of λ that the conservation measures can conceivably induce.

The coherence criteria we have discussed

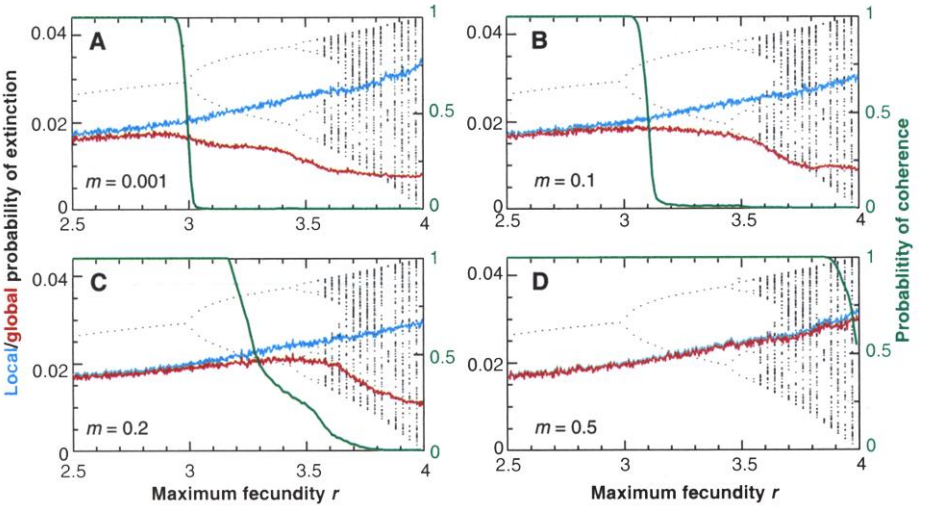

Fig. 3. Risk of extinction. Local and global extinction probabilities in the logistic metapopulation model (with equal coupling). Each panel corresponds to a different fraction, m, of dispersing individuals. (**A**) $m = 0.001$, (**B**) $m = 0.1$, (**C**) $m = 0.2$, and (**D**) $m = 0.5$. Local (blue) and global (red) extinction probabilities are shown as functions of the maximum fecundity r. As in Fig. 1, the graphs are superimposed on the bifurcation diagram for the logistic map. The local extinction probability increases with r because oscillations in abundance increase in amplitude as r increases. Where the blue and red curves do not overlap, global extinction is less likely than local extinction in individual patches. For sufficiently small dispersal fractions, there is always (at least a small) difference between local and global extinction probabilities (because the basin of attraction of the coherent attractor does not encompass all initial conditions). For sufficiently large dispersal fractions, local and global extinction probabilities are the same for all initial conditions, regardless of the value of r. In each panel, the green curve (corresponding to a slice of the top left panel of Fig. 2) gives the probability of coherence. A substantial difference between local and global extinction probabilities occurs only when the probability of coherence is small.

can be applied equally well if we wish to exterminate rather than preserve a species; in such cases, it would be advantageous to promote rather than prevent synchrony (*8*). Our results can thus be used to develop improved methods for controlling or eradicating introduced species. In the case of human infectious diseases (*37, 38*), vaccination campaigns have had a dramatic effect on the spatial synchrony of epidemics (*8, 9*); conditions such as criterion 3 may allow us to identity immunization strategies that synchronize epidemics and thereby increase the probability of global eradication.

References and Notes

1. S. L. Pimm, *Nature* **393**, 23 (1998).
2. W. F. Laurance, R. O. Bierregaard Jr., Eds., *Tropical Forest Remnants: Ecology, Management, and Conservation of Fragmented Communities* (Univ. of Chicago Press, Chicago, 1997).
3. I. A. Hanski, M. E. Gilpin, Eds., *Metapopulation Biology: Ecology, Genetics, and Evolution* (Academic Press, San Diego, CA, 1997); I. Hanski, O. Ovaskainen, *Nature* **404**, 755 (2000).
4. R. Levins, *Bull. Entomol. Soc. Am.* **15**, 237 (1969).
5. J. H. Brown, A. Kodric-Brown, *Ecology* **58**, 445 (1977).
6. M. Heino, V. Kaitala, E. Ranta, J. Lindstrom, *Proc. R. Soc. London Ser. B* **264**, 481 (1997).
7. B. Blasius, A. Huppert, L. Stone, *Nature* **399**, 354 (1999).
8. D. J. D. Earn, P. Rohani, B. T. Grenfell, *Proc. R. Soc. London Ser. B* **265**, 7 (1998).
9. P. Rohani, D. J. D. Earn, B. T. Grenfell, *Science* **286**, 968 (1999).
10. P. Beier, R. F. Noss, *Conserv. Biol.* **12**, 1241 (1998).
11. A. Gonzalez, J. H. Lawton, F. S. Gilbert, T. M. Blackburn, I. Evans Freke, *Science* **281**, 2045 (1998).
12. F. Courchamp, T. Clutton-Brock, B. Grenfell, *Trends Ecol. Evol.* **14**, 405 (1999).
13. P. A. Stephens, W. J. Sutherland, *Trends Ecol. Evol.* **14**, 401 (1999).

14. The simplest population models predict total population density at discrete time intervals. The densities of individuals in successive generations ($t = 0, 1, 2,\ldots$) are obtained by iterating a discrete map,

$$x^{t+1} = F(x^t) \tag{4}$$

where x^t denotes the population density at time t. The spatial distribution of many species can be represented as a metapopulation, i.e., a network of relatively isolated local patches, within which individuals reproduce and among which some individuals disperse (*3*). The example emphasized in the main text is a single-species metapopulation model. If the population density in patch i at time t is x_i^t, then the dynamical equations are

$$x_i^{t+1} = \sum_{j=1}^{n} m_{ij} F(x_j^t) \qquad i = 1,\ldots,n, \tag{5}$$

where m_{ij} is the proportion of individuals from patch j that disperse to patch i, n is the number of patches, and F is the reproduction function as in Eq. 4. $M = (m_{ij})$ is the dispersal matrix (*15*). The logistic metapopulation is defined by Eqs. 5 with F the normalized logistic map (*39–41*)

$$F(x) = rx(1 - x) \tag{6}$$

where r is the maximum fecundity.

15. In our illustrative example, the dispersal matrix M has one of two simple forms. For equal coupling, a proportion m from each patch disperses uniformly among the other $n - 1$ patches, and a proportion $1 - m$ does not disperse. Formally

$$m_{ij} = \begin{cases} m/(n-1) & \text{if } i \neq j \\ 1 - m & \text{if } i = j \end{cases} \tag{7}$$

For nearest neighbor coupling on a one-dimensional ring, a fraction $m/2$ from each patch disperses to each of the two nearest neighbor patches and the remaining fraction $1 - m$ does not disperse. Thus, the dispersal matrix is

$$M = \begin{pmatrix} 1-m & m/2 & 0 & \cdots & m/2 \\ m/2 & 1-m & m/2 & \cdots & 0 \\ 0 & m/2 & 1-m & \cdots & 0 \\ \vdots & \vdots & \vdots & \ddots & \vdots \\ m/2 & 0 & 0 & \cdots & 1-m \end{pmatrix} \tag{8}$$

For both these simple cases, the dispersal matrix M is symmetric ($m_{ij} = m_{ji}$), meaning that the proportion of individuals from patch i that disperse to patch j is the same as the proportion from patch j that disperse to patch i. This need not be the case, however, and the matrix M could in general have a very complicated structure. For example, it may be easier to disperse in one direction (e.g., because of prevailing winds or altitude changes), and dispersal rates may be much higher in some areas than in others (e.g., because of local weather or topography). Our results do not depend on the dispersal matrix being symmetric.

16. The metapopulation is in a coherent state at time t if the population density in each patch is the same ($x_i^t = x_j^t$ for all i and j at time t). A sequence of patch densities that satisfy Eqs. 5 is a coherent solution if the metapopulation is in a coherent state at all times.
17. The probability of coherence is determined by the total volume of the basins of attraction of all coherent attracting solutions (*16*) of Eqs. 5. For each r and m in Fig. 2, we estimated this probability on the basis of a sample of 10^4 initial conditions. The probability of coherence was taken to be the proportion of the 10^4 trajectories that were coherent to within 10% after 10 iterations of Eqs. 5 (see caption to Fig. 2). A random sample of initial conditions was used because the basin boundaries of different attractors may be very complicated (so Monte Carlo sampling of initial conditions is most effective). This simple approach can be applied to any spatial population model.
18. To obtain the extinction probabilities in Fig. 3, we subjected the system, with probability 0.1 each year, to a "global event." Such events were modeled as additive, normally distributed noise with mean 0 and standard deviation 0.35. If, after adding this global noise, the population density in patch i was $x_i \leq 0$, then we set $x_i = 0$ and the species was considered to be extinct in patch i. After each global extinction ($x_i = 0$ for all i), all patches were restarted with random population density, as in the computation of coherence probabilities (*17*). The process was repeated for 50,000 iterations for each r value.

19. J. C. Allen, W. M. Schaffer, D. Rosko, *Nature* **364**, 229 (1993).
20. G. D. Ruxton, *Proc. R. Soc. London Ser. B* **256**, 189 (1994).
21. L. Stone, *Nature* **365**, 617 (1993).

22. An eigenvalue λ of a matrix M is subdominant if, among all eigenvalues of M, λ has the second largest magnitude. In general, two or more distinct eigenvalues can be subdominant. However, we refer to "the" subdominant eigenvalue λ because only the magnitude of λ is important for our results.

23. The Lyapunov exponent of a single patch map F is the exponential rate of divergence of population densities that are initially nearly equal and can be written (*41*)

$$\mu = \lim_{T\to\infty} \frac{1}{T} \sum_{t=0}^{T-1} \log|F'(x^t)| \tag{9}$$

An n-dimensional dynamical system can have n Lyapunov exponents (*41*), which give rates of divergence or convergence of nearby trajectories in all phase-space directions. If the dispersal matrix M is diagonalizable and $(1,1,\ldots,1)$ is an eigenvector of M with eigenvalue 1, then a straightforward computation (*42*) shows that, along a coherent solution (*16*), the metapopulation (Eq. 5) has n Lyapunov exponents given by

$$\mu_k = \mu + \log|\lambda_k| \qquad k = 1,\ldots,n, \tag{10}$$

where μ is the Lyapunov exponent of the single-patch map F on the associated single patch trajectory and the λ_k are the eigenvalues of M.

24. J. A. J. Metz, R. M. Nisbet, S. A. H. Geritz, *Trends Ecol. Evol.* **7**, 198 (1992).
25. In this note, we sketch some of the key ideas involved in establishing criteria 1, 2, and 3. Mathematical details are given elsewhere (*42*). Trajectories of the single-patch map are coherent solutions (*16*) of the corresponding metapopulation if and only if $(1, 1, \ldots, 1)$ is an eigenvector of M with eigenvalue 1; we assume this because we are interested in spatial generalizations of nonspatial population models. Locally (in phase space), the system will relax to coherence if all but the maximum Lyapunov exponent are negative; thus, we require (*23*)
$$\mu + \log|\lambda| < 0 \quad (11)$$
where λ is the subdominant (*22*) eigenvalue of M. This is criterion 1. (To obtain the boundaries of the blue regions in Fig. 1, we approximated Eq. 9 with a finite sum.) A few special cases of this local result (for particular types of matrices M) have been noted previously (*26–30*). All these previous results are subsumed by criterion 1. From Eq. 9, it is clear that if $r = \sup_x|F'(x)|$, then $\mu(x^0) \leq \log r$ regardless of the initial condition x^0. Consequently
$$\log r + \log|\lambda| < 0 \quad (12)$$
is sufficient to guarantee that the system relaxes to coherence globally (in phase space). This is criterion 3. In general, more than one coherent solution of Eqs. 5 may be locally stable, so different initial states may be attracted to different coherent solutions. If the single-patch map always has a unique attractor [which is true, in particular, for the logistic map (*40*)], then condition 3 guarantees that the corresponding coherent attractor of the metapopulation is the unique attracting solution of Eqs. 5. Both the local and global coherence criteria can be established rigorously and do not depend on M being diagonalizable; elsewhere (*42*), we show this in detail and rigorously characterize the dispersal patterns of systems that admit locally stable coherent oscillations (in practice, this includes all ecologically relevant models).
26. K. Kaneko, *Phys. Rev. Lett.* **63**, 219 (1989).
27. A. Hastings, *Ecology* **74**, 1362 (1993).
28. R. V. Solé, J. G. P. Gamarra, *J. Theor. Biol.* **193**, 539 (1998).
29. J. A. L. Silva, M. L. De Castro, D. A. R. Justo, *Bull. Math. Biol.* **62**, 337 (2000).
30. T. Bohr, M. H. Jensen, G. Paladin, A. Vulpiani, *Dynamical Systems Approach to Turbulence* (Cambridge Univ. Press, Cambridge, 1998), §4.1.1.
31. The logistic metapopulation model that we used for the figures is merely the simplest idealized case. However, the results for the logistic reproduction function are representative for many systems (the sequence of bifurcations is generic in a broad class of dynamical systems). In addition, simulations show that our results are not substantially affected by demographic or environmental stochasticity (local noise).
32. Our analytical results, Eqs. 1 to 3, can be generalized in a number of important ways (*42*). They apply, essentially as stated, to metapopulations involving multiple species, age structure, external (explicitly time-dependent) forcing, and other realistic features. The key technical point behind these extensions is that our derivations of the coherence conditions do not depend on the single-patch map (F) being one-dimensional. If F is multidimensional, then in the local criteria 1 and 2, the Lyapunov exponent μ is simply replaced by the maximal Lyapunov exponent of the multidimensional single-patch map; in the global criterion 3, the maximum reproductive rate [$r = \sup_x|F'(x)|$] is replaced by the maximum of the matrix norm of the Jacobian derivative of F. Similar conditions can also been obtained for systems involving continuous space and/or continuous time.
33. It is an immediate consequence of condition 1 that locally stable, nonchaotic solutions of the single-patch map are always locally stable as coherent solutions (*16*) of the metapopulation. The reason is that $|\lambda| < 1$ for any ecological model (*42*) and $\mu \leq 0$ for nonchaotic dynamics (equilibria, cycles, or quasi-periodic oscillations), so condition 1 always holds. For coherent chaos, local stability depends on the dispersal pattern. For any given $\mu > 0$, there are dispersal matrices such that $e^{\mu}|\lambda| < 1$ and others such that $e^{\mu}|\lambda| > 1$. In Fig. 1, we see that (for the logistic metapopulation with equal coupling) if the fraction of dispersing individuals (m) is sufficiently large, then coherent solutions are always locally stable, even at the extreme of $r = 4$.
34. A. Hastings, C. L. Hom, S. Ellner, P. Turchin, H. C. Godfray, *Annu. Rev. Ecol. Syst.* **24**, 1 (1993).
35. S. Ellner, P. Turchin, *Am. Nat.* **145**, 343 (1995).
36. The subdominant (*22*) eigenvalue λ is a function only of the dispersal matrix M, not the within-patch map F. Consequently, even if we cannot obtain any reasonable approximation of F for a real system, we can use estimates of changes in λ to predict roughly how conservation measures such as corridors affect coherence (and extinction) probabilities. Small changes in λ typically do not yield large changes in the total volume of the basins of attraction of coherent oscillations.
37. R. M. Anderson, R. M. May, *Infectious Diseases of Humans: Dynamics and Control* (Oxford Univ. Press, Oxford, 1991).
38. D. J. D. Earn, P. Rohani, B. M. Bolker, B. T. Grenfell, *Science* **287**, 667 (2000).
39. R. M. May, *Nature* **261**, 459 (1976).
40. P. Collet, J.-P. Eckmann, *Iterated Maps on the Interval as Dynamical Systems*, vol. 1 of *Progress in Physics* (Birkhäuser, Basel, 1980).
41. J. Guckenheimer, P. Holmes, *Nonlinear Oscillations, Dynamical Systems, and Bifurcations of Vector Fields*, vol. 42 of *Applied Mathematical Sciences* (Springer-Verlag, Berlin, 1983).
42. D. J. D. Earn, S. A. Levin, in preparation.
43. A. Hastings, K. Higgins, *Science* **263**, 1133 (1994).
44. We thank A. Balmford, S. Balshine, B. Grenfell, R. Johnstone, L. Stone, and L. Worden for helpful discussions and comments on a preliminary manuscript. We were supported by the Natural Sciences and Engineering Research Council of Canada (NSERC), the Royal Society, the Sloan Foundation, and the David and Lucile Packard Foundation (award number 8910-48190).

20 June 2000; accepted 3 October 2000

PSD-95 Involvement in Maturation of Excitatory Synapses

Alaa El-Din El-Husseini,[1]* Eric Schnell,[2]* Dane M. Chetkovich,[1,3] Roger A. Nicoll,[2] David S. Bredt[1]†

PSD-95 is a neuronal PDZ protein that associates with receptors and cytoskeletal elements at synapses, but whose function is uncertain. We found that overexpression of PSD-95 in hippocampal neurons can drive maturation of glutamatergic synapses. PSD-95 expression enhanced postsynaptic clustering and activity of glutamate receptors. Postsynaptic expression of PSD-95 also enhanced maturation of the presynaptic terminal. These effects required synaptic clustering of PSD-95 but did not rely on its guanylate kinase domain. PSD-95 expression also increased the number and size of dendritic spines. These results demonstrate that PSD-95 can orchestrate synaptic development and are suggestive of roles for PSD-95 in synapse stabilization and plasticity.

Despite the central role for synapses in neuronal function, mechanisms underlying synapse formation remain incompletely understood. Recently, proteins containing PDZ motifs have been proposed as molecular scaffolds for receptors and cytoskeletal elements at synapses (*1–4*). The prototypical PDZ protein, postsynaptic density–95 (PSD-95/SAP-90), is a membrane-associated guanylate kinase (MAGUK) concentrated at glutamatergic synapses (*5*, *6*). PSD-95 may participate in synapse development because it clusters at synapses before other postsynaptic proteins (*7*), and because *discs large*, a PSD-95 homolog in *Drosophila*, is necessary for proper development of larval neuromuscular junctions (*8*). Despite numerous studies it remains uncertain whether PSD-95 participates in synapse development in mammals. Targeted disruption of PSD-95 in mice does not alter synaptic structure (*9*), possibly because three other MAGUKs and dozens of other PDZ proteins occur at brain synapses. This molecular redundancy has obscured understanding of functions for PSD-95 and other PDZ proteins in the brain.

We overexpressed PSD-95 to help define its roles (*10*). Green fluorescent protein (GFP)–tagged versions of PSD-95 target faithfully to postsynaptic sites in hippocampal neurons, despite being overexpressed 5 to 10 times above endogenous levels (*11*, *12*). To evaluate the effects of PSD-95 on synaptic development, we analyzed cultures at early developmental stages, day in vitro (DIV) 10 to 12, and noted an increase of glutamate receptor subunit–1 (GluR1) immunofluorescence at postsynap-

[1]Department of Physiology, [2]Department of Cellular and Molecular Pharmacology, and [3]Department of Neurology, University of California, San Francisco 94143, USA.

*These authors contributed equally to this work.
†To whom correspondence should be addressed: E-mail: bredt@itsa.ucsf.edu